Available online at www.sciencedirect.com
ScienceDirect
Journal of Sound and Vibration 323 (2009) 757–771
JOURNAL OF SOUND AND VIBRATION
www.elsevier.com/locate/jsvi

Non-uniform impact excitation of a cylindrical bar

Baruch Karp[a,*], Avraham Dorogoy[b], Zonggang Wang[b]

[a]*Department of Mechanical Engineering, Ben-Gurion University of the Negev, P.O.B. 653, Beer-Sheva 84105, Israel*
[b]*Faculty of Mechanical Engineering, Technion—Israel Institute of Technology, Haifa 32000, Israel*

Received 9 September 2008; received in revised form 31 December 2008; accepted 8 January 2009
Handling Editor: C.L. Morfey
Available online 7 February 2009

Abstract

An experimental and numerical study of a non-uniform impact excitation of a circular bar is reported. In experiments, nine strikers with different contact area were accelerated against a circular bar. Axial surface strain of the impacted bar was measured at several distances from the impinged end to include the near and the far fields. The same experimental conditions were solved numerically using a commercial finite element code. It was demonstrated that the far-field response is insensitive to both the size and the form of the striker's colliding end. The distance at which such insensitivity is set is estimated to be approximately one and a half bar diameters.

1. Introduction

The question of sensitivity of a waveguide's response to the form of an end excitation has attracted much attention for already several decades. Asymptotical and numerical studies of response of a bar to an impact suggested that "if any truly significant effects due to non-uniform end loading of the bar are present, they must occur at propagation distances which, as an upper bound, are less than 20 bar diameters" (Ref. [1], p. 473). That statement has extended previous asymptotic results reported by Fox and Curtis [2], Jones and Norwood [3], and Curtis [4] in the context of sensitivity to mixed or pure nature of the end excitation. That bound of 20 bar diameters was set due to the limits of validity of the asymptotic method used rather than from any result showing that the distance cannot be smaller than that.

A similar result is obtained for a transient response of a plate in plane strain by Sinclair and Miklowitz [5]. More recent works investigate wave propagation in a waveguide subjected to non-uniform end excitation (e.g., Refs. [6,7]), however these did not present explicit data enabling one to deduce on the extent of the region beyond which various forms of excitation generate the same dynamic response.

Using finite element analysis, Meng and Li [8] suggested that for a split Hopkinson pressure bar setup (SHPB), the upper bound on the sensitivity to non-uniformity of the striker form can be as small as 1.5 diameters from the excited end, provided the average pressure in the bar's cross-section is the criterion for

*Corresponding author. Tel.: +972 4 829 2237.
E-mail address: bkarp@bgu.ac.il (B. Karp).

0022-460X/$ - see front matter © 2009 Elsevier Ltd. All rights reserved.
doi:10.1016/j.jsv.2009.01.005

presence of non-uniformity effect. That estimation is profoundly lower than the standard upper bound of 10–20 diameters.

Sparse experimental studies bring further evidence for negligible effect of non-uniform excitation at distances which are lower than 10 bar diameters. Flynn and Frocht [9] used the photoelastic method to compare the effect of uniform, circular and concentrated loading. Bell [10] compared the effect of excitation generated by projectiles having various contact forms with the same contact area concluding with "… impacts of small hollow cylinders of the same area as the solid rod demonstrated that beyond the first half-diameter the experimental results were insensitive to the major changes in the spatial distribution of loading at the impact face." (p. 351). Miles [11], putting emphasis on the experimental aspects of end excitation, provide another example for conditions under which the effect of non-uniform excitation is limited to a region much smaller than 20 widths of the plate.

Bell's comment inspired repetition of experimental and numerical investigation of the effect of non-uniformity of the striker at the School of Civil and Environmental Engineering, Nanyang Technological University, Singapore. That investigation was limited to four strikers, which have an identical contact area but different form as pointed by Bell. The results of that investigation are not yet reported.

In the present communication a further experimental investigation of the effect of non-uniform excitations is reported with an emphasis on the estimation of the size of the near field region where the form of the excitation does have a significant effect. Here, the effect of both the form and the contact area at the impinged end were examined. Particularly, we wish to demonstrate the insensitivity of the surface strain far from the excited end to those two properties of the excitation and to estimate the distance which can be considered as "far enough".

The experimental setup consisted of a basic SHPB with an incident bar (the impacted bar) specially instrumented to record surface axial strain at several distances along the bar. The variability of the form of excitation of the incident bar was achieved by nine different strikers (one flat, four bore type, and four pin type) having different contact areas (ratio of up to two). The strain signals were analyzed on the basis of one-dimensional theory of wave propagation in a bar, according to which the form of the signal is trapezoidal with height related to the striker velocity V by the relation

$$\varepsilon = \frac{\sigma}{E} = \frac{V}{2C} \tag{1}$$

where ε and σ are the axial strain and stress, E is Young's modulus, and C the velocity of longitudinal waves in a bar. That trapezoidal form of the signal is referred to as *first-order response*.

The purpose of the experiments was to estimate the distance from the impinged end at which the response of the incident bar is not sensitive to the form and to the magnitude of the contact area of the striker—the excitation. An attempt has been made to keep the temporal properties of the repetitive experiments as similar as possible, with the spatial form of the exciting load as a controlled variable. Finite element analysis was used to simulate the experiments from which the interior strains were extracted. These results were used to further explore the sensitivity of the interior regions of the incident bar to the striker's form.

The main result emerging from this study is that the distance at which the first-order response of the bar is insensitive to both, the contact area and its form, is about 1.5 times the bar diameters. That result for nine strikers was found to be in good agreement with previous results for the four different strikers examined on different systems (bars having 2.5 times larger diameter). These results are also consistent with analytical predictions based on evanescent waves in bars and with a similar experimental finding in a beam-like waveguide [12].

In Section 2 the experimental setup, procedure, and numerical scheme are detailed. Results are given in Section 3 followed by discussion in Section 4 where a well-known analytical solution to a waveguide problem is used to interpret the experimental results. Section 5 is devoted to the summary of the conclusions obtained.

2. Experimental details and modeling

In the design of the experimental setup the immediate aim was to examine the differences in surface strains along the bar due to impacting strikers having different contact area shapes. That dictated a system which is able to measure and to record the surface strain response in the near and far fields of the incident bar.

2.1. The setup

The experimental equipment is based on a standard SHPB system (Fig. 1) located at the Dynamic Fracture laboratory at the Faculty of Mechanical Engineering at the Technion. The setup consisted of an incident bar made of PH-17 Steel (static yield at 900 MPa, Poisson's ratio $\nu = 0.27$, mass density $\rho = 7655\,\mathrm{kg/m^3}$, $C = 5190\,\mathrm{m/s}$), with diameter $D = 19.05\,\mathrm{mm}$ and length 1000 mm and a striker made of the same material and diameter with length 242 mm. Seven couples of diametrically cemented collinear strain gauges were attached to the incident bar at distances of 4.7, 14.1, 28.6, 76.1, 152.7, 311, and 550 mm from the excited end, $x = 0$ (corresponding to non-dimensional distances $x' \equiv x/D$ of 0.247, 0.74, 1.5, 4.0, 8.0, 16.3, and 28.9), and designated as *stations* 1–7, respectively. Stations 1–6 were equipped with strain gauges having gauge length of 0.2 mm while the gauge length at station 7 was of 2 mm. The strain gauges were sampled simultaneously at the rate of 2 MHz/16-bit with a gain of 200. The reading of each strain gauge couple was averaged to cancel out any possible bending of the incident bar.

Three basic striker configurations which differ only in their contact area and end shape were used (Fig. 2); one standard flat striker (denoted by F), a bore configuration consisted of four strikers (denoted by B1–B4), and a pin configuration consisted of four strikers (denoted by P1–P4). The dimensions of all nine strikers' contact area are detailed in Table 1. The eight-shaped strikers' heads were designed to make four couples to have the same contact area. Each striker was accelerated by an air pressure gun with velocity measured through a slot at the gun exit by a four-diode arrangement.

It is worth noting that several previous papers report on evolution of a signal as it propagates along the bar (e.g., Ref. [13]). Nevertheless, these works are dedicated to the investigation of the dispersion phenomena, thus the measurements are taken only at stations remote from the impinged end.

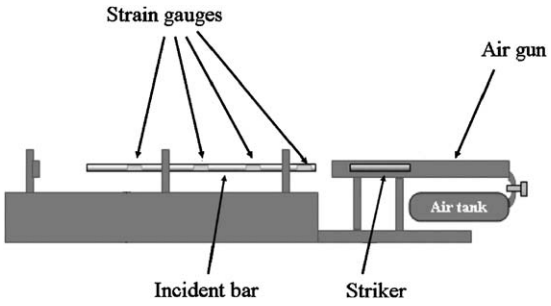

Fig. 1. Schematic view of the experimental setup used in the experiments.

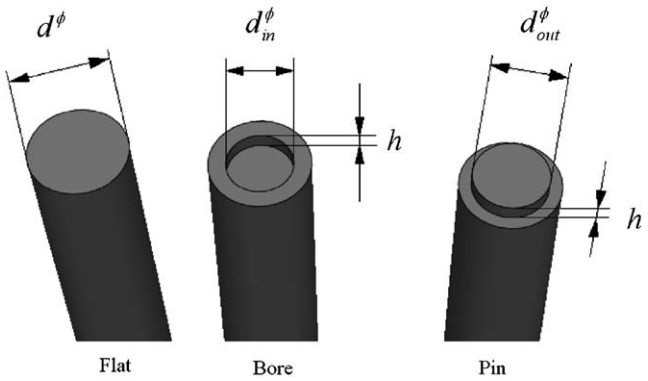

Fig. 2. Configuration of the three types of striker heads. $d = 19.05\,\mathrm{mm}$, $h = 3\,\mathrm{mm}$. Bore diameter d_{in}, pin diameter d_{out}, and contact area of each are detailed in Table 1.

Table 1
The pin and bore diameters and contact area for the nine strikers.

Flat striker	Pin striker	Contact area	d_{out} (mm)	Bore striker	Contact area	d_{in} (mm)
F (area = 285)	P1	250	17.84	B1	250	6.68
	P2	220	16.75	B2	220	9.10
	P3	190	15.55	B3	190	11.00
	P4	160	14.26	B4	162	12.50

Area is in units of mm^2.

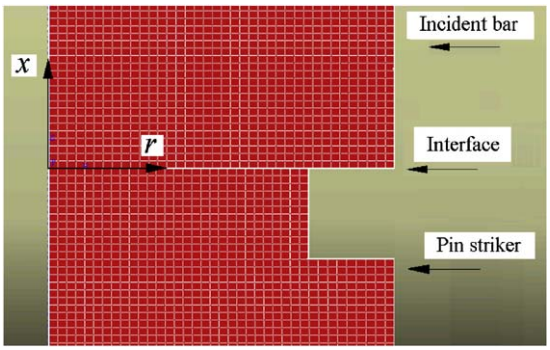

Fig. 3. Typical mesh configuration of CAX4R axisymmetric elements of size ~0.25 mm at the contact areas between the striker and the incident bar. Pin striker is shown. Note that the left side is the radial symmetry line.

2.2. Experiments

The experiments consisted of few repetitive firings of each striker with two target velocities of 7 and 18 m/s. Three firings were made with each striker to verify repeatability. The maximal velocity is expected to generate stress of magnitude of 610 MPa in the striker with the smallest contact area. This assures the material to remain within the elastic limit.

2.3. Finite Element Model

The above experiments were simulated with the commercial finite element code ABAQUS Explicit version 6.7. A transient linear elastic simulation was performed. Due to the radial symmetry an axisymmetric model was used. The model uses a 4-node bilinear axisymmetric quadrilateral element (CAX4R). A fine mesh of element size 0.25 mm which exhibits a numerical convergence was used for all simulations. The mesh of the impinged bar consists of 152,000 elements while the mesh of the striker P4 (for example) consists of 36,484 elements. The mesh at the contact region between the striker and the bar for striker P4 is shown in Fig. 3. In the simulation the striker was given an initial velocity of 17.8 m/s and frictionless contact was applied between the striker and the bar. The simulation lasted for 250 micro-seconds, allowing time for the arrival of the pulse head to the distance of 1.3 m. The pulse itself lasts about 120 micro-seconds.

3. Results

Fig. 4 shows typical recordings at stations 1, 2, and 7 for the case of a flat striker given a velocity of 16.5 m/s. The strain values are left in voltage units as measured. Recordings at the same stations induced by strikers P4 and B4 with a slightly higher velocity are shown in Figs. 5 and 6, respectively. The first-order trapezoidal signal characterizes the strain-time response at all stations. The agreement between the average amplitude of the signal at station 7 and the prediction of the one-dimensional theory in Eq. (1) can be judged from Fig. 7. In

Fig. 7 the averaged amplitude at station 7 for 27 experiments is shown as a function of striker's velocity. From Eq. (1) the relation between the strain and the impact velocity should be linear with a slope equal to $1/2C$. The linear best-fit for the experimental results leads to $C = 5242$ m/s, which is within 2% off the nominal data of 5190 m/s.

The deviation of average strain at station 1 from the prediction of Eq. (1) for the non-uniform strikers, as shown in Figs. 5 and 6, is expected in view of several previous results (e.g., Refs. [8–10]). Similar deviation, though smaller in its magnitude, for a flat striker is notable in Fig. 4 and was not expected. A flat striker ideally should generate a uniform wave from the very end of the bar (for frequencies low enough, of course). That deviation of strain at station 1 from the strain at station 7 occurred in all experiments with a flat striker (15 experiments). In some experiments the amplitude at station 1 is higher than at station 7 though in most of them it is lower. That deviation is attributed to some not yet identified imperfection in the bars' geometry or alignment affecting only the extremely sensitive region of the near field.

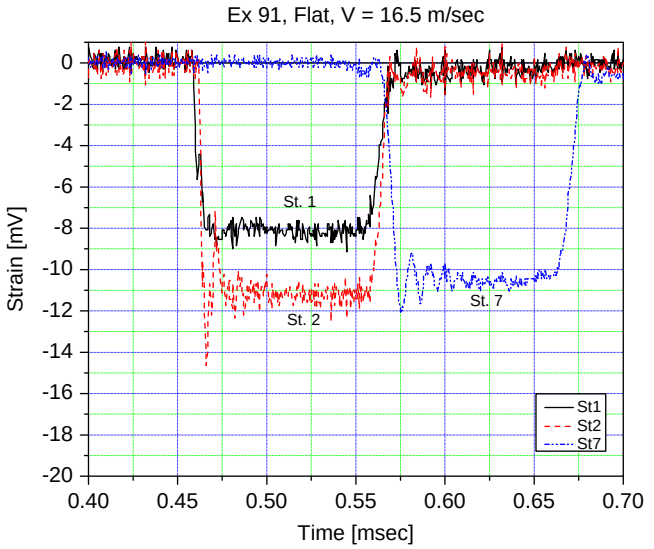

Fig. 4. Strain gauge recordings at stations 1, 2, and 7 induced by F striker with velocity of 16.5 m/s.

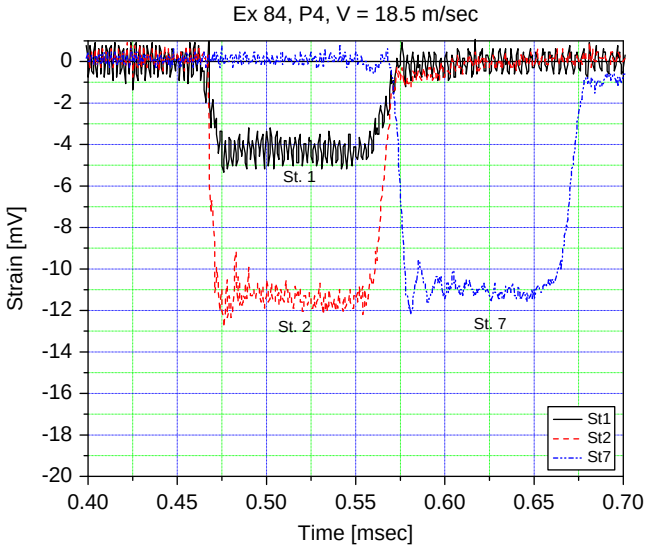

Fig. 5. Strain gauge recordings at stations 1, 2, and 7 induced by P4 striker with velocity of 18.5 m/s.

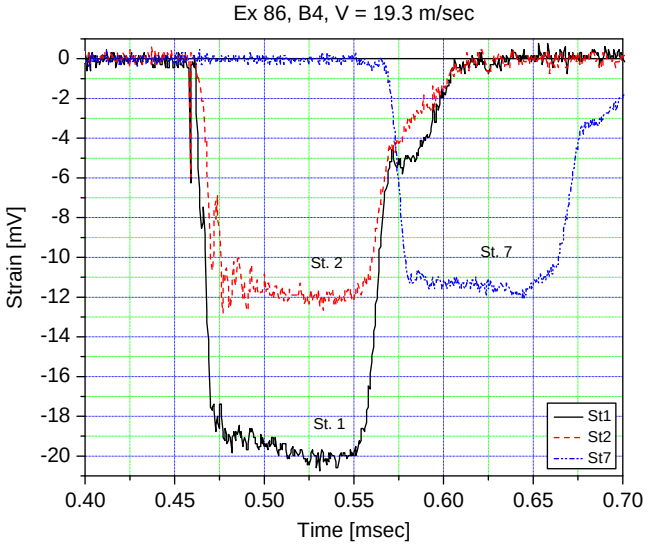

Fig. 6. Strain gauge recordings at stations 1, 2, and 7 induced by B4 striker with velocity of 19.3 m/s.

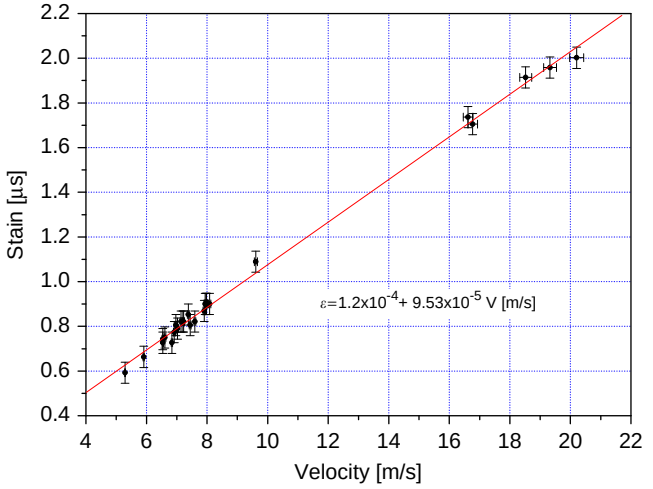

Fig. 7. Average strain at station 7 for 27 experiments with various strikers at different striker's velocity. The linear best fit and its expression are added to the graph.

Further examination of these plots reveals that the amplitudes of the recordings at stations 2 and 7 for all three strikers are essentially the same. That result is common to all strikers and considered as the central observation in our context. Additional demonstration of an almost identical signal at stations 2–6 is shown in Fig. 8 reproducing signals recorded for a striker B1 impinged at a velocity of 7.6 m/s.

The last observation to be noted in Figs. 4–6 relates to second-order effects that distinguish the various strikers. It is evident from Figs. 6 and 8 that bore strikers have two noticeable characteristics different from the flat and the pin strikers. One is a trailing edge of the trapezoidal signal of bore strikers having a turn at the end of the signal. That change in slope is identical at all stations, occurs for all bore strikers (Figs. 6 and 8), and can be noticed also in other experimental instances (e.g., Ref. [13], Figs. 3–7). The second observation relates to the absence of the regular sinusoidal variation of the signal at the head of the trapezoidal form in the bore strikers at station 7. That sinusoidal response, interrupted after a particular time, is typical to flat and pin strikers, Figs. 4 and 5, and is thoroughly explained by Fox and Curtis [2] for a uniform step excitation. These two second-order features of the dynamic response are out of the scope of the present study.

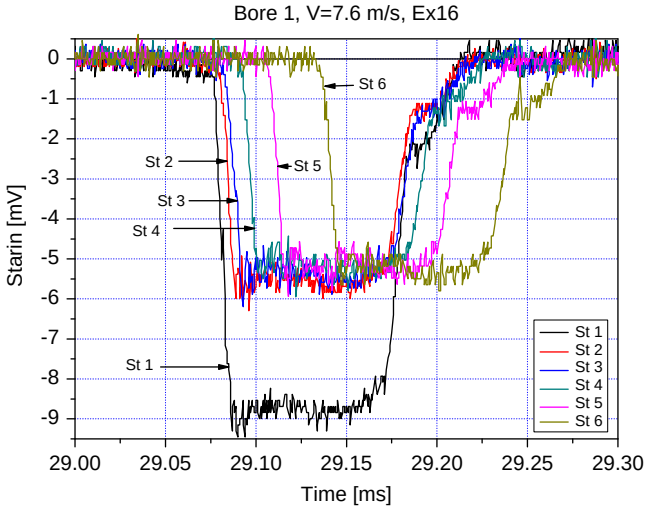

Fig. 8. Recordings at stations 1–6 for striker B1 impinged at a velocity of 7.6 m/s.

For a more convenient comparison of the first-order response we draw strain recordings for all nine strikers at stations 1 and 5 (station 5 is typical for the far-field response) on the same chart in Fig. 9a and b, respectively. The signals are shifted arbitrarily along the time axis to provide a clearer view of each signal on the same graph. It can be observed from Fig. 9b that there is only a minor difference in amplitude between all nine results for station 5. This small deviation is found to result from the slightly different striker velocities (7 ± 1 m/s) scaling of which according to Eq. (1) gives identical first-order response (to within a few percent) for all nine strikers at that particular station 5 and stations 3, 4, 6, and 7 as well. It is apparent that the recordings at station 1 (Fig. 9a) differ markedly, way beyond the possible correction for the actual velocity of the strikers. A comparison of the signals at station 2 with the signals at station 7 in Figs. 4–6 suggests that beyond station 2 all the signals would be identical to that predicted by the first-order theory (Eq. (1)). That may lead to the conclusion that station 1 lies well within the affected zone (affected by the form of the striker) while station 2 lies outside of that zone.

From Fig. 9a it can be concluded that the bore strikers induce higher strain at the surface close to the impinged end. Pin strikers, on the other hand, generate lower strains. That different response dies out showing only negligible effect "far enough" from the impinged end. The distance at which the effect can be considered as negligible is examined in the next section.

Numerical simulation for the same experiments has been performed to further investigate the interior response of the impinged bar. The close agreement between the experimental and numerical results for a striker velocity of 17 m/s is exemplified in Fig. 10. Here the time and strains are scaled to the time required for a wave to cross one diameter of the bar, D, and to the strain at infinity, according to the relations

$$t' = \frac{t}{D/C} \quad \varepsilon' = \frac{\varepsilon}{\varepsilon_\infty} = \varepsilon\frac{2C}{V} \tag{2}$$

where ε' is the scaled strain. Fig. 10 shows the numerical and the experimental results for the surface response at station 1 for three strikers—flat, P4, and B4. The observed 5–10% discrepancy can be attributed to experimental and numerical errors, especially due to extreme sensitivity to the exact location of the strain gauge within the near field (as can also be seen from Figs. 12 and 13).

In Figs. 11a, b the relative strains ε' (according to Eq. (2)) within the cross-section at stations 1 and 2 are plotted for strikers B1, B4 and P1, P4, respectively. The curves generated from an average of approximately 60 readings at times during which the signal is passing through the particular point. Due to typical fluctuation of the signal, as seen in Figs. 4–6 and 8–10, it is not expected that the accuracy of the average will be better that 5%. Up to that value of error, it turns out that the internal distribution of strain at station 2 is close to uniform

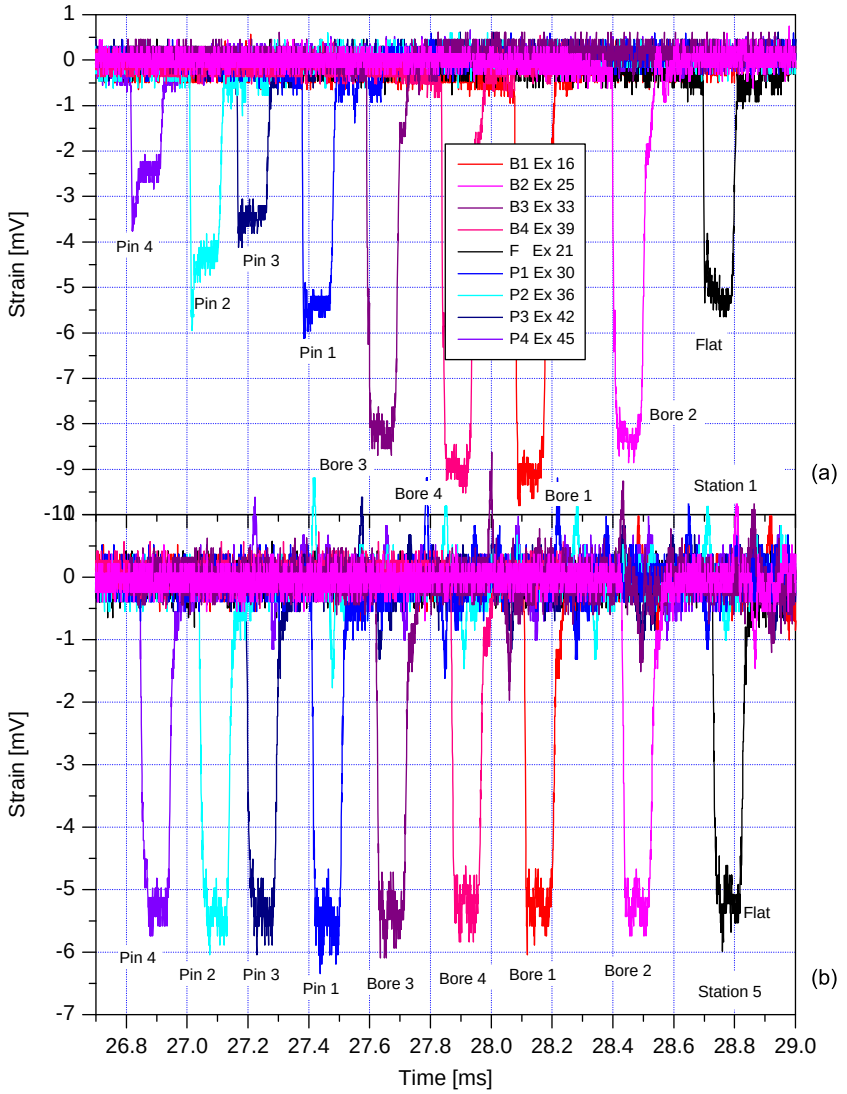

Fig. 9. Recordings at stations 1 and 5 for all nine strikes at approximate velocity of 7 m/s. (a) Station 1 and (b) station 5.

agreeing well with surface recordings (Figs. 4–6) according to which the response at station 2 is almost identical to the response at infinity.

4. Discussion

The experimental results for the surface strains obtained with the various strikers give a rough estimation for the extent of the effect of different striker forms as judged based on the first-order response. That distance is between station 1 ($x' = 0.25$) and station 2 ($x' = 0.74$). However, the numerical result at the interior regions of the rod, shown in Fig. 11b, suggest that that distance is between station 2 ($x' = 0.74$) and station 3 ($x' = 1.5$). For a more conclusive estimation of the extension of the affected zone, further analysis of the numerical results was performed.

To more accurately estimate the extent of the affected zone numerical results for the surface strain were plotted versus the distance from the impinged end. To emphasize the deviation from the first-order response given by Eq. (1), the average amplitudes of the relative strains ε', defined in Eq. (2), are plotted in Fig. 12 versus the normalized distance x'. Results for only four strikers B1, B4, P1, and P4, are shown. Due to

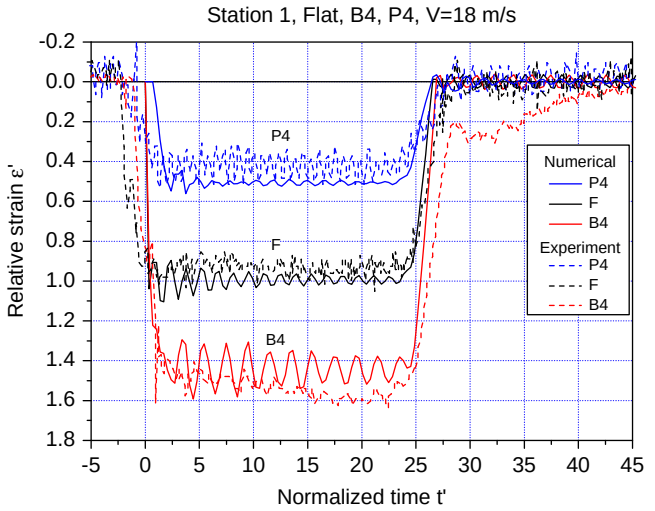

Fig. 10. Comparison between experimental and numerical results at station 1 for three types of strikers: flat, P4, and B4. The axes are normalized time and relative strain. Strikers' velocity is 18 m/s.

averaging process of the fluctuating signals the accuracy of these curves is not expected to be better than 5%, which is the same as for the curves in Fig. 11 and in Fig. 13. Apparently, beyond the distance of $x' \approx 0.8$ all strikers produce the same response. The distance beyond $x' = 0.8$ is thus designated on the graph as an *unaffected zone*, meaning that up to the first-order response that zone is unaffected by the form and the size of the contact surface at the impinged end. That value of $x' = 0.8$ agrees well with the experimental result of strain at station 2 which is almost indistinguishable from the strain at more distant stations. The near zone, estimated to be limited to $x' < 0.8$, is extremely sensitive to the details of the excitation thus referred to as an *affected zone*.

Experimental results of the relative strain at station 1 are shown in Fig. 12 as well. It is evident that the experimental and the numerical results for pin strikers lie within a reasonable error range. The bore strikers, on the other hand, exhibit extremely large departure between the numerical and the experimental results. Large discrepancy between the numerical and the experimental results found to exist also for a flat striker where the deviation at station 1 from the theoretical result of 1.0 scatters between 0.7 and 1.1. The exact explanation of that apparent discrepancy remains to be explored. It is estimated here that its origin lies in some experimental inaccuracy (misalignment, curvature of the surfaces), and numerical inaccuracy (especially the averaging process of a non-uniform response) which, for some reason, are more prominent in flat and bore strikers.

Fig. 13 traces the relative axial strain at the axis of the bar, $r = 0$, as calculated numerically from the FE simulations for the same four strikers, recordings of which are shown in Fig. 12. As expected, the magnitude of the signals for bore and pin strikers are inverted between $r = 0$ and a, where a is the bar radius. The convergence of all signals to within $|\varepsilon' - 1.0| \approx 0.04$ at $x' \approx 1$ can be observed, though convergence to $\varepsilon' = 1.0$ occurs only at $x' \approx 1.5$. That distance is larger than the convergence distance of $x' \approx 0.8$ obtained above in Fig. 12, judged upon the surface strain. Due to inherent inaccuracy of about 5% in deriving the curves themselves (as mentioned above), there is no point in making much more accurate estimation. This is especially valid given these estimations are based on a limited sample of the cross-section field ($r = 0$, $r = a$) and for only four types of strikers in Figs. 11–13 and eight strikers in Fig. 9.

The result emerging from the experiments and from the numerical simulations shown here, according to which the extent of the affected zone is only one and a half bar diameters, stands much shorter to the one commonly used in practice (see recent review in Ref. [14]). Yet it agrees well with experimental results as hinted in a note by Bell [10] and with the results obtained in recent investigation at Nanyang Technological University (to be reported). It is of interest here to examine whether that result could be expected from the theory of waveguides and to what degree it agrees with the experiments. The examination

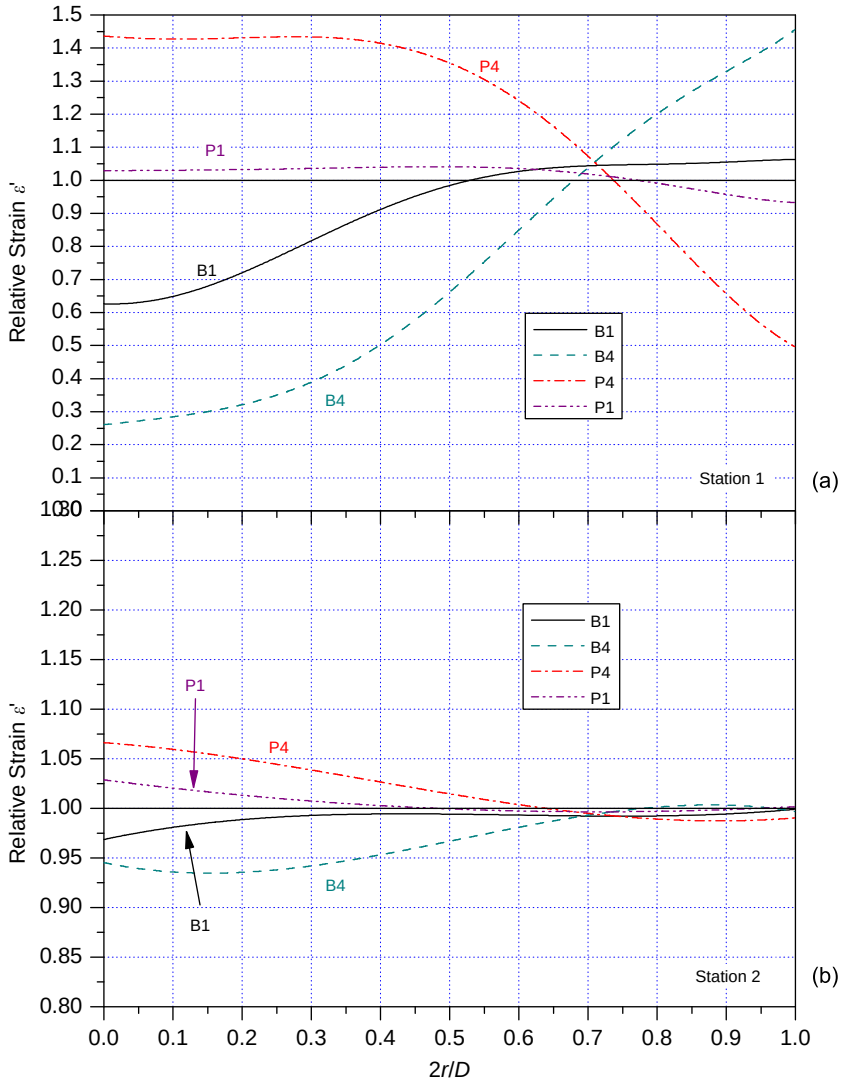

Fig. 11. Numerical results for the axial strain variation with radius at stations 1 and 2 (normalized to the strain at infinity). (a) Station 1 and (b) station 2 (note the different strain scaling).

will be based on general properties of waveguide dynamics without actually solving for the exact conditions encountered in the experiments. In particular, the questions raised are what is the origin of the observed different response within the affected zone and whether it is possible, based on waveguide dynamics, to estimate its size.

Analytical solution of elastic wave propagation in a waveguide is commonly written in the form of separation of variables given for the displacement field $\mathbf{u}$ by (e.g., Ref. [15])

$$\mathbf{u}(x,r,t)=\sum_{n=1}^{N}A_n\mathbf{U}_n(r)\,\mathrm{e}^{\mathrm{i}(\xi_n x-\omega t)}+\sum_{n=N+1}^{\infty}A_n\mathbf{U}_n(r)\,\mathrm{e}^{\mathrm{i}\xi_n x}\mathrm{e}^{-\mathrm{i}\omega t} \tag{3}$$

where ω is the circular frequency, n stands for the wave modes with complex valued amplitude A_n, real, complex, or imaginary wavenumber ξ_n, and $\mathbf{U}_n(r)$ is the associated cross-sectional profile for both velocity components in the axial and radial directions (x, r), respectively. The separation into two sums made here to emphasize the distinction between the finite number of N propagating modes having real valued wavenumbers

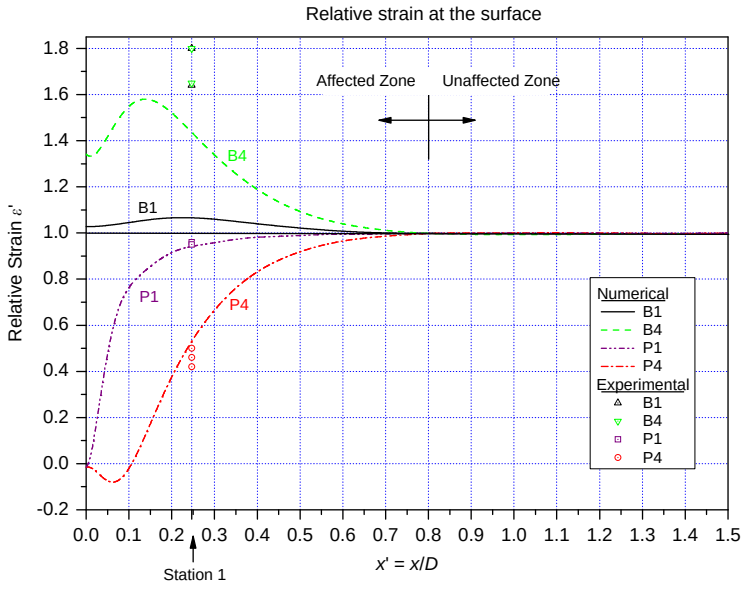

Fig. 12. Numerical results for the axial strain at the surface (normalized to the strain at infinity) for the flat, P4, and B4 strikers at various distances from the end of the input bar.

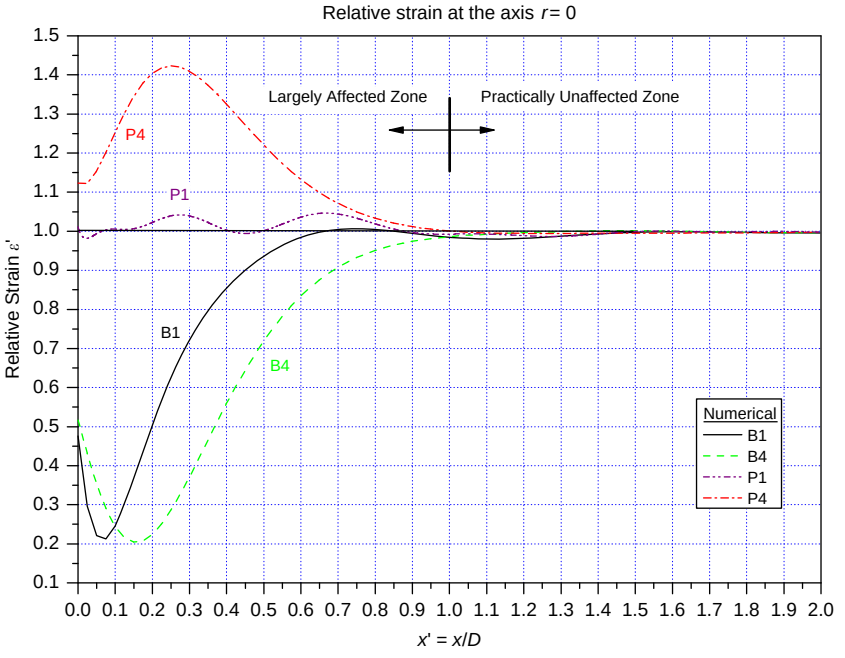

Fig. 13. Numerical results for the axial strain at the bar axis (normalized to the strain at infinity) for the P1, P4, B1, and B4 strikers at various distances from the end of the input bar.

(the first sum) and the evanescent waves characterized by complex and imaginary wavenumbers. It is evident from Eq. (3) that for complex and imaginary wavenumbers the amplitude decays exponentially along the axial direction x (the wavenumbers leading to exponential growth are excluded on a physical ground). The largest attenuation distance is dictated by the wavenumber having the smallest imaginary part. The distance at which

only 1% of the original amplitude is remained is given

$$l_{0.01} = \frac{|\ln(0.01)|}{\mathrm{Min}\{|\mathrm{Im}[\xi]|\}} \tag{4}$$

and can be considered as a typical *upper bound* for the attenuation distance. Here, $\mathrm{Min}\{|\mathrm{Im}[\xi]|\}$ is the *attenuation constant*.

Harmonic steady-state analysis of a waveguide response, in a form of Eq. (3), together with the aid of Fourier's theory provides a powerful tool for understanding a transient response in waveguides. Frequency maps derived from the Pochhammer–Chree equations for bars (and Rayleigh–Lamb equations for plates, e.g. Ref. [15]), assigning the valid wavenumbers ξ_n for each frequency ω, predict that sensitivity of the waveguide response to the form of the excitation can be attributed to two phenomena. One is the different partition of energy among the N propagating modes generated in the case when the frequency range allows for more than one propagating mode [16]. The second origin for different responses of differently distributed end excitation is attributed to evanescent waves [17].

More than one propagating wave mode can exist at frequencies above the first cutoff frequency. Assuming only axisymmetric modes generated, any load with frequency lower than that cutoff frequency will generate only the fundamental mode, i.e., $N = 1$. For a bar with a Poisson's ratio of 0.27, the non-dimensional cutoff frequency is approximately $\Omega_{\mathrm{cutoff}} = 3.7$ (Ref. [18], p. 327), with the non-dimensional frequency defined as

$$\Omega \equiv \frac{a}{C_T}\omega \tag{5}$$

where a is the radius of the bar, C_T the transversal wave velocity, and ω the angular frequency. If the excitation contains frequencies above that cutoff frequency, and the energy is partitioned differently among the possible modes for different strikers, the resulting displacement field will be different all the way down the waveguide due to the nature of wave propagation (due to various combinations of the first sum in Eq. (3)). In a resent study by Karp [19] it was found that the same energy partition takes place for different *moderately non-uniform*, harmonic excitations, resulting in a similar far-field response for this family of different spatial forms of excitations even in the high-frequency regime. That means that form variation of the excitation within some limits does not alter the energy partition among the available wave modes. For material properties and geometry of the bar used in the experiment, the first cutoff frequency obtained from Eq. (5) is

$$f_{\mathrm{cutoff}} = \frac{\omega_{\mathrm{cutoff}}}{2\pi} = \frac{C_T}{2a\pi}\Omega_{\mathrm{cutoff}} \approx 200\ \mathrm{kHz} \tag{6}$$

Transient response of colliding bars cannot be generally limited to low frequencies below that first cutoff frequency. Follansbee and Frantz [20] and Tyas and Watson [21] have shown that typical impact in a SHPB system consists mainly of the fundamental first mode of the waveguide. Fox and Curtis [2], on the other hand, confirm experimentally that traces of second mode in pressure-induced excitation do exist.

To estimate the frequency content in a strain signal a Fourier analysis (FFT) of typical results is performed on recordings at stations 7 and 1 for three experiments with strikers F, B4, and P4. Fig. 14 shows the FFT of the signals at station 7 of the three experiments while Fig. 15 shows FFT of a signal at station 1 of the same experiments. It can be observed that the signals at station 7 for all three strikers (F, B4, and P4) have the same frequency spectrum with negligible frequencies beyond 150 kHz. The frequency spectrum at station 1, as shown in Fig. 15, is different for the three strikers in two ways. At low frequencies the amplitudes are different, reflecting the different amplitude of the trapezoidal response. At high frequencies, between 100 and 200 kHz, the difference is noticeable as well, though limited to amplitudes much smaller than the height of the trapezoid. Yet, at both stations the frequencies conveying most of the energy are below 100 kHz. That frequency is below the first cutoff frequency given in Eq. (6) and hence, most of the energy is conveyed by frequencies in the region where only one propagating mode can be generated at each frequency. Therefore, it is expected that if any propagating mode other than the first is excited, its contribution to the signal will be at least 10 times smaller than the contribution of the first mode at low frequencies. Indeed, the amplitude of the oscillations at the head of the trapezoidal signal is about 10 times smaller than the height of the signal itself. Yet, these small amplitude waves cannot explain the large deviation in strain at the first station. Moreover,

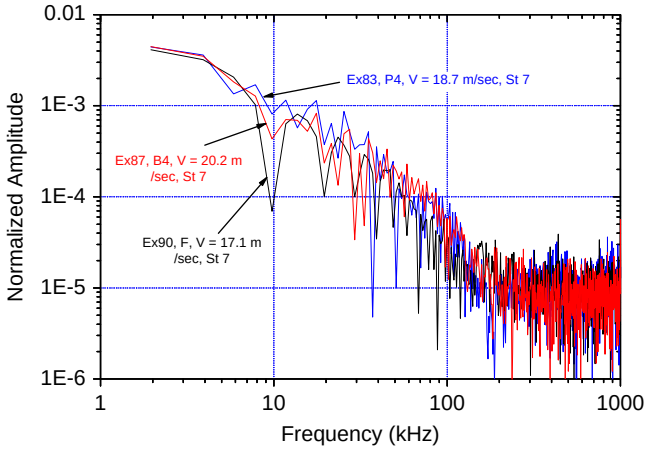

Fig. 14. Typical frequency spectrum of a strain signal for strikers F, B4, and P4 at station 7.

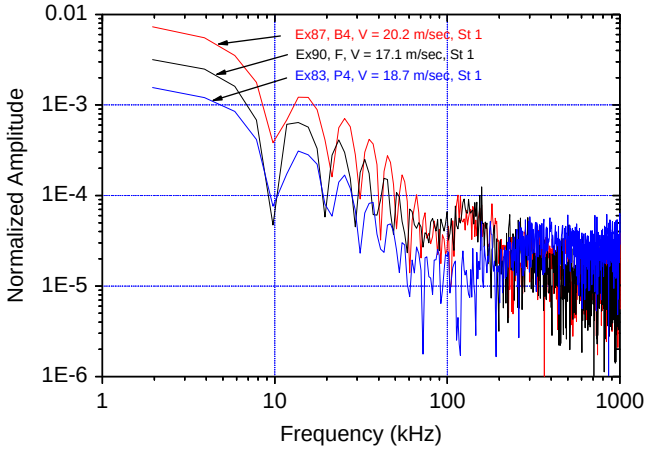

Fig. 15. Typical frequency spectrum of a strain signal for strikers F, B4, and P4 at station 1.

propagating modes are not attenuated at such a high rate to die out at the second or the third stations as turned out to be the case for all strikers and experiments.

We turn now to examine the possible contribution of the evanescent waves to the deviation of the strain at the first station from the strain at further stations. Generation of the evanescent waves depends on the exact boundary condition and is said to be excited to compensate for the difference between the form of the propagating modes and the form of excitation itself. It is natural, therefore, to expect generation of different evanescent waves for differently distributed loads over the excited bar end.

Due to the decaying nature of these waves, the different response should be limited to the close vicinity of the excited end, usually termed the *near field*. No strict and general upper bound on the size of the near field could be established due to the possibility of inducing evanescent waves with very large decay distances at high frequencies close to cutoff frequencies (Ref. [22] for plates and Ref. [23] for bars).

To estimate the bounds on decay distance in our system we use the Pochhammer–Chree solution for the steady-state response of a semi-infinite bar with Poisson's ratio of 1/3 given by Zemanek [23]. Typical upper frequencies in the signal (as seen in Figs. 14 and 15) of $f = 100$, 150 kHz correspond to non-dimensional frequencies $\Omega = 1.9$, 2.8, respectively. These in turn, from Zemanek [23], give the smallest attenuation constants of $a\xi \approx 2.5$, 1.7, respectively. By Eq. (4), for the value of $a\xi = 1.7$, the attenuation of any field to 1% of its original value at $x = 0$ is at a distance of 1.35 times the bar diameter. Some minor variation on that estimation is expected for materials with different Poisson's ratios (Ref. [24]). This shows a very close match

between the distances at which the strain signal converges to the strain at infinity as found from experiments, numerical simulations, and analytical solution of the attenuation range of the evanescent waves.

We may conclude that the evanescent waves are the origin for the different amplitudes at the first station for different strikers. Given that, the upper bound for decay of these waves is dictated by the evanescent mode having the smallest imaginary part in the wavenumber. In the region of frequencies below 150 kHz, that value is approximately 1.7 giving a decay distance of about 1.4 times the bar diameter. That analytical bound agrees well with the numerical and the experimental results obtained here. That result is comparable to a similar estimation of the transient response of a beam with rectangular cross-section [12] where the affected zone for a transient wave reflection from a built-in end was found to extend up to one width of the beam.

5. Concluding remarks

The effect of various shapes of the contact area of the striker on the transient response of a bar has been examined experimentally and numerically. Axial strains were measured by standard gauges located at various distances from the impinged end and extracted from numerical simulations performed with a FE code. It was found that the first-order response of the bar is insensitive to the form of the excitation at distances greater than one and half diameters from the excited end. The meaning of this insensitivity is as follows: based on the first-order response at stations located beyond 1.5 times the bar diameter, one cannot tell which of the strikers were impinged on the bar while the velocity of the striker can be extracted based on Eq. (1) whatever the form or the magnitude of the area of the contacting interface. That region of one and a half diameters from the impinged end is the affected zone where the bar response is extremely sensitive to the form and the size of the excitation and is much smaller than commonly assumed.

It is evident that the size of the affected zone depends on the type of striker used and the exact location at the cross-section upon which the attenuation is judged. Therefore, the estimation obtained here cannot be considered as a rigorous upper bound on the size of the affected zone. Yet, waveguide dynamics support that estimation which is of a comparable size as in the static case [25].

The design of the form of the strikers used in this investigation had mainly theoretical interest for examination of the form effect. Yet, the forms examined might have some practical implications. Pin-type strikers can be considered as simulating a standard compression SHPB experiment when the diameter of the specimen is smaller than the diameter of the bars (e.g., Ref. [26]) or any other non-uniform excitation form (e.g., Ref. [27]). Bore-type strikers have some similarity to the form of bars in shear punch dynamic tests (e.g., Ref. [28]) and the ring compression test (e.g., Ref. [29]). The tension test in the SHPB system also involves excitation that cannot be considered as uniform both for the system bars (e.g., Ref. [30]) and for the sample itself (e.g., Ref. [31]). Furthermore, the results obtained here might be of practical interest for the SHPB system design with large diameter bars (e.g., Ref. [32]) where the requirement to locate strain gauges at distances larger than 10 diameters of the bar is difficult to achieve.

Acknowledgments

One of the authors (B.K.) wishes to express his thanks to the kind hospitality of the Faculty of Aerospace Engineering, Technion, Haifa. The availability of experimental equipment and technicians at the Dynamic Fracture Laboratory of Prof. Daniel Rittel at the Faculty of Mechanical Engineering at the Technion is acknowledged.

References

[1] L.W. Kennedy, O.E. Jones, Longitudinal wave propagation in a circular bar loaded suddenly by a radially distributed end stress, *Journal of Applied Mechanics ASME* 36 (1969) 470–478.

[2] G. Fox, C.W. Curtis, Elastic strain produced by sudden application of pressure to one end of a cylindrical bar. II. Experimental observations, *Journal of the Acoustical Society of America* 30 (1958) 559–563.

[3] O.E. Jones, F.R. Norwood, Axially symmetric cross-sectional strain and stress distributions in suddenly loaded cylindrical elastic bars, *Journal of Applied Mechanics ASME* 34 (1967) 718–724.

[4] C.W. Curtis, Propagation of an elastic strain pulse in semi-infinite bar, in: N. Davids (Ed.), *International Symposium on Stress Wave Propagation in Materials*, Interscience Publishers Inc., New York, 1960, pp. 15–43.
[5] G.B. Sinclair, J. Miklowitz, Two nonmixed symmetric end-loadings of an elastic waveguide, *International Journal of Solids and Structures* 11 (1975) 275–294.
[6] Y.Y. Kim, C.R. Steele, End effects and time-harmonic longitudinal wave propagation in semi-infinite solid cylinder, *Journal of Applied Mechanics ASME* 56 (1989) 334–346.
[7] A. Tyas, A.J. Watson, A study of the effect of spatial variation of load in the pressure bar, *Measurement Science and Technology* 11 (2000) 1539–1551.
[8] H. Meng, Q.M. Li, An SHPB set-up with reduced time-shift and pressure bar length, *International Journal of Impact Engineering* 28 (2003) 677–696.
[9] P.D. Flynn, M.M. Frocht, On Saint-Venant's principle under dynamic conditions, *Experimental Mechanics* 1 (1) (1961) 16–20.
[10] J.F. Bell, The experimental foundations of solid mechanics, in: S. Flugge (Ed.), *Mechanics of Solids*, Vol. VIa/1, in *HNBK der Physik*, Springer, New York, 1973.
[11] A.W. Miles, Shock-front loading method for studies in dynamic photoelasticity, *Experimental Mechanics* 16 (9) (1976) 349–355.
[12] B. Karp, D. Rittel, D. Durban, Health monitoring of joints using dynamic end effects, *Journal of Sound and Vibration* 312 (1-2) (2008) 257–272.
[13] J.C. Gong, L.E. Malvern, D.A. Jenkins, Dispersion investigation in the split Hopkinson pressure bar, *Journal of Engineering Materials and Technology—Transactions of ASME* 112 (1990) 309–314.
[14] B. Karp, Dynamic version of Saint-Venant's principle—historical account and recent results, *Nonlinear Analysis* 65 (2005) e931–e942.
[15] J.D. Achenbach, *Wave Propagation in Elastic Solids*, North-Holland Pub. Co, Amsterdam, 1973.
[16] R.D. Gregory, I. Gladwell, The reflection of a symmetric Rayleigh–Lamb wave at the fixed or free edge of plate, *Journal of Elasticity* 13 (1983) 185–206.
[17] J.L. Rose, *Ultrasonic Waves in Solid Media*, Cambridge University Press, Cambridge, 1999.
[18] D. Royer, E. Dieulesaint, *Elastic Waves in Solids I*, Springer, Berlin, 1996.
[19] B. Karp, Generation of symmetric Lamb waves by non-uniform excitations, *Journal of Sound and Vibration* 312 (1-2) (2008) 195–209.
[20] P.S. Follansbee, C. Frantz, Wave propagation in the split Hopkinson pressure bar, *Journal of Engineering Materials and Technology* 105 (1983) 61–66.
[21] A. Tyas, A.J. Watson, Experimental evidence of PC strain variations in elastic cylinder, *Experimental Mechanics* 40 (3) (2000) 331–337.
[22] B. Karp, D. Durban, Evanescent and propagating waves in prestretched hyperelastic plates, *International Journal of Solids and Structures* 42 (2005) 1613–1647.
[23] J. Zemanek Jr., An experimental and theoretical investigation of elastic wave propagation in a cylinder, *Journal of the Acoustical Society of America* 51 (1972) 265–283.
[24] M. Onoe, H.D. McNiven, R.D. Mindlin, Dispersion of axially symmetric waves in elastic rods, *Journal of Applied Mechanics ASME* 29 (1962) 334–346.
[25] R.W.M. Little, S.B. Childs, Elastostatic boundary region problem in solid cylinders, *Quarterly Applied Mathematics* 25 (1967) 261–274.
[26] Z. Li, J. Lambros, Determination of the dynamic response of brittle composites by the use of the split Hopkinson pressure bar, *Computer Science and Technology* 59 (1999) 1097–1107.
[27] T.S. Lok, P.J. Zhau, G. Lu, Using the split Hopkinson pressure bar to investigate the dynamic behaviour of SFRC, *Magazine of Concrete Research* 55 (2) (2003) 183–191.
[28] W. Dabboussi, J.A. Names, Modeling of ductile fracture using the dynamic punch test, *International Journal of Mechanical Sciences* 47 (2005) 1282–1299.
[29] R.S. Hartley, T.J. Cloete, G.N. Nurick, An experimental assessment of friction effects in the split Hopkinson pressure bar using the ring compression test, *International Journal of Impact Engineering* 34 (2007) 1705–1728.
[30] T. Nicholas, Tensile testing of materials at high rates of strain, *Experimental Mechanics* 21 (5) (1981) 177–185.
[31] M. Sasso, G. Newaz, D. Amodio, Material characterization at high strain rate by Hopkinson bar tests and finite element optimization, *Material Science and Engineering A* 487 (2008) 289–300.
[32] P.J. Zhao, T.S. Lok, A new method for separating longitudinal waves in a large diameter Hopkinson bar, *Journal of Sound and Vibration* 257 (2002) 119–130.